

Simple Approach for Building High Transconductance Paper-Based Organic Electrochemical Transistor (OECT) for Chemical Sensing

Adil Ait Yazza, Pascal Blondeau, and Francisco J. Andrade*

Cite This: *ACS Appl. Electron. Mater.* 2021, 3, 1886–1895

Read Online

ACCESS |



Metrics & More



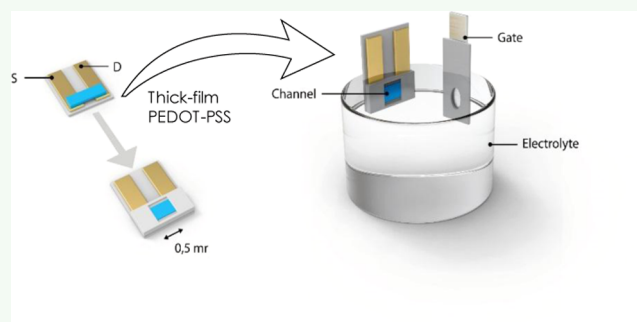
Article Recommendations



Supporting Information

ABSTRACT: Organic electrochemical transistors (OECTs) have attracted great interest in the last few years as biochemical sensors due to their outstanding analytical performance, versatility, stability, and easiness of fabrication. While thin-film OECTs have been studied extensively, their manufacturing still presents some challenges. This report presents a simple approach for developing OECT using a paper substrate and a thick-film approach that shows outstanding performance. The channel is hand-made by dip pen deposition of the conducting polymer poly(3,4-ethylenedioxythiophene) doped with polystyrene sulfonate (PEDOT:PSS). This allows reproducible channel thickness in the order of 6 μm , well above the conventionally used values. This device displays a high transconductance that exceeds 40 mS and an on-to-off current ratio of 3.8×10^3 comparable or superior to the state-of-the-art paper-based OECTs. The advantages of this approach are illustrated with the detection of H_2O_2 and glucose, obtaining sensitivities above 1.5 mA/dec. This simplified approach and high sensitivity may help to extend the use of the OECT-based sensors, particularly in the distributed and point-of need applications.

KEYWORDS: thick-film transistors, dip pen, OECT, hydrogen peroxide, glucose detection



1. INTRODUCTION

Ever since the pioneering work of White et al. more than three decades ago,¹ the use of organic electrochemical transistors (OECT) has been growing at an increasing rate. Today, OECTs play major roles in electrochromic displays,² logic gates,³ bioelectronics,⁴ and biochemical sensors,⁵ among others. A major milestone for their development was the use of aqueous-based conducting polymer (CP) solutions, such as PEDOT:PSS.⁶ This material shows very good performance, simplifies the manufacturing processes, and has allowed the development of transistors on a wide variety of materials such as paper,^{7,8} plastics,⁹ elastomers,^{10–12} fabrics,¹³ etc. This has led to the fabrication of wearable and embedded electronic components. Significant efforts to improve the OECT performance,¹⁴ understand their mechanisms,¹⁵ and model their behavior¹⁶ are being recently made. OECTs offer significant advantages in chemical and biochemical sensing, including a simple setup, power amplification of the signal, versatility, and biocompatibility. As a result, during the last few years, the number of communications using OECTs in (bio)chemical sensing has outpaced other approaches, such as field-effect devices. OECT sensors for the detection of ions, small biomolecules (e.g., glucose),¹⁷ dopamine,¹⁸ uric acid,¹⁹ ascorbic acid,²⁰ sarcosine,²¹ proteins,²² nucleic acids and living cells,²³ and even whole viruses²⁴ have been reported. Currently, the range of applications is also expanding toward

low-cost and wearable platforms for an increasing number of targets.²⁵

An OECT is typically made of three electrodes, source (S), drain (D), and gate (G) (Figure 1). The S and D are connected by a CP channel that, upon application of a voltage (V_d), allows the flow of a current (I_d). As in any transistor, the principle of operation of an OECT is that an input voltage on the gate produces a modulation of the current in the channel (I_d), which is the output signal. In both organic field-effect transistors (OFETs) and OECTs, the gate and the channel are separated by a dielectric layer. However, in OECTs, the dielectric layer is formed by an ionically conductive electrolyte solution that allows the free exchange of ions. This feature is key for the unique mechanism of the OECTs. It has been shown that the PEDOT:PSS films show an ionically modulated electronic conductivity, i.e., the electronic charge carriers in the PEDOT (holes) are stabilized by the electrostatic effect of the sulfonate groups in the PSS. When ions migrate into the channel driven by V_g , they alter the electrostatic effect of the

Received: February 3, 2021

Accepted: March 18, 2021

Published: March 29, 2021



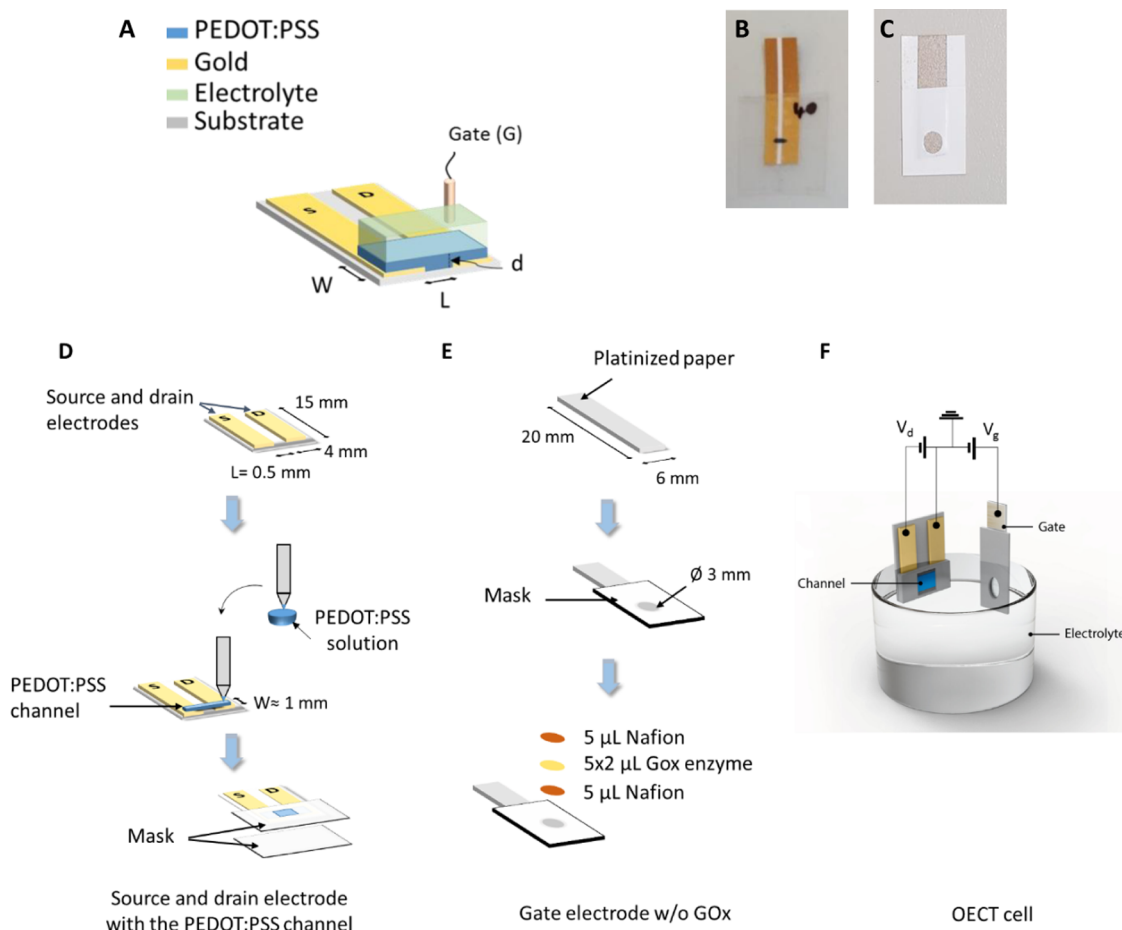


Figure 1. (A) Schematic of an OEET, where W is the width, L is the length, and d is the thickness of the channel. (B) Source/drain electrodes and PEDOT:PSS channel. (C) Platinum gate electrode. (D) Drawing of the PEDOT:PSS channel. (E) Construction of the platinum gate electrode. (F) Schematic of the measurement cell.

sulfonate groups, which leads to changes in the hole concentration and mobility in the PEDOT phase, thus affecting I_d . Because of this mechanism, I_d becomes a function of V_g with a proportionality measured by the transconductance of the system (g_m)

$$g_m = \frac{\partial I_d}{\partial V_g} \quad (1)$$

Transconductance is a critical parameter in chemical sensing, because it is related to the amplification of the signal and, ultimately, the sensitivity of the technique.²⁶ While significant work is currently focused on increasing the transconductance through the modification of channel materials, a straightforward way to optimize g_m is through the manipulation of the channel geometry. Unlike field-effect transistors, which show a two-dimensional (2D) surface-limited capacitance, the hydrophilic and porous PEDOT:PSS channel creates a volumetric, three-dimensional (3D) capacitance²⁷ that allows OEETs to display transconductances significantly higher than other transistors.²⁸ It is well known that the transconductance is directly related to the channel dimensions

$$g_m \propto \frac{W \times d}{L} \quad (2)$$

where W (width), L (length), and d (thickness) are the channel characteristics as shown in Figure 1. Therefore, there

is a direct way to enhance the transconductance by increasing the channel thickness.²⁹ Nevertheless, the response time (τ) is also affected by the channel thickness¹⁵

$$\tau \propto d\sqrt{WL} \quad (3)$$

As a result, optimization of the OEETs has been traditionally characterized by a trade-off between transconductance and response time. For this reason, thickness has been usually kept below 1 μm . With channels ranging from tens to several hundreds of nanometers, transconductances in the order of 5 mS and response times in the millisecond range have been reported.³⁰ Thus, transconductances are still significantly higher than in other transistors, while response times are low enough for many applications. Rivnay et al., for example, successfully recorded human brain activity using two PEDOT:PSS OEETs with channel thicknesses of 230 and 870 nm.²⁹ Since the vast range of applications are based on these types of devices, fundamental studies of the OEETs have been traditionally kept within this range. There are significant efforts to improve the response time by minimizing the effects of diffusion, such as the modifications of the channel composition,³¹ internal ion reservoirs,³² ionic liquids,³³ etc. In all cases, channel thickness has been kept under the micrometer range, and applications of OEETs with channel thickness above 1 μm are scarce.³⁴

In chemical and biochemical sensing, the response time is often controlled by the kinetics linked to the recognition

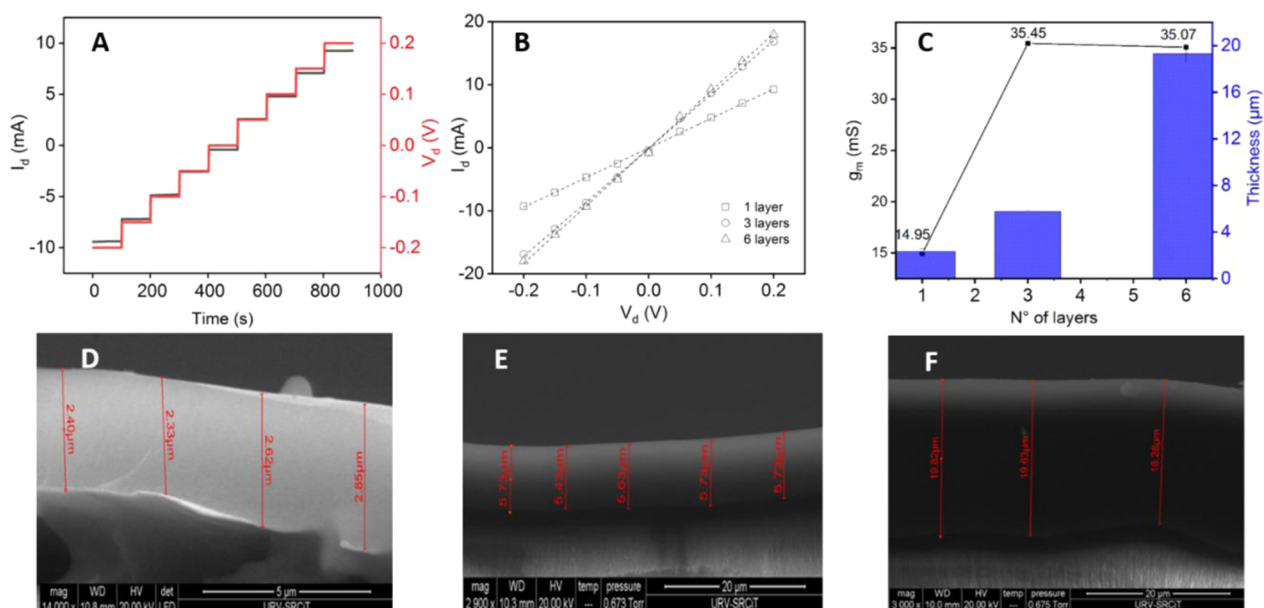


Figure 2. (A) Time plot of I_d for a channel with one PEDOT:PSS layer as V_d changes from -0.2 to 0.2 V. (B) $I_d - V_d$ characteristics of three dry channels with one, three, and six layers of PEDOT:PSS tested without gating and without electrolyte. (C) Transconductance and channel thickness as a function of number of layers deposited by dip pen method. The error bars represent the standard deviation of the thickness measured at three different positions. ESEM cross sections of three PEDOT:PSS channels having (D) one layer, (E) three layers, and (F) six layers.

events. In these situations, the optimization is mostly based on maximizing the transconductance, to enhance the sensitivity. Therefore, it is worth questioning whether using thicker channels—beyond the traditional nanometer range limit—might be a valid approach to maximize the analytical response. The answer is not straightforward, since phenomena linked to ion migration, film hydration, swelling, etc. may be negatively affecting the performance of the system.

In this work, we explore the characteristics of a thick-film OECT when applied to the determination of hydrogen peroxide, a molecule that is present in a plethora of biochemical sensing schemes. In the last few years, we have studied the use of a Pt electrode coated with a layer of Nafion for the potentiometric determination of H_2O_2 and the construction of biosensors.³⁵ OECTs for the detection of hydrogen peroxide and the generation of glucose sensors using Pt and composite materials for the gate have also been reported.^{36–39} Thus, this work will show the advantages of the thick-film platforms, such as the simplicity of construction of paper-based devices, to generate chemical sensors and biosensors. Analytical characterization of the thick-film sensor for hydrogen peroxide and proof of principle of a glucose sensor are presented.

The results show that a film with a thickness of several microns can be reproducibly made by a simple dip pen approach, thus easing the manufacturing process of these sensors. It is shown that using a Ag/AgCl gate electrode, a value of transconductance of 35 mS can be reached, which is close to the highest values reported up to date for this type of devices. In addition, when using a Pt/Nafion gate electrode, a highly sensitive detection of peroxide can be obtained, with sensitivities of 2.1 mA/decade. Therefore, this work opens new ways for the simple construction and operation of powerful, low-cost, and highly sensitive OECT chemical sensors.

2. MATERIALS AND METHODS

2.1. Reagents and Materials. All chemicals used were of analytical grade and were purchased from Sigma-Aldrich (Merck, Spain). And a 3–4% aqueous solution of high-conductivity-grade PEDOT:PSS was used for making the conductive films. Fresh H_2O_2 standard solutions were prepared daily from a commercial 30% (v/v) stock. A solution of 5% wt Nafion in aliphatic alcohols and water (15–20% water) was used to make the gate electrode. Glucose oxidase (from *Aspergillus Niger* Type X-S) lyophilized powder, 100–250 kU/g, was used to prepare a stock solution in deionized water (20 mg/mL). Phosphate-buffered saline (PBS 0.1 M at pH 7.4) was prepared by dissolving 0.100 M Na_2HPO_4 , 0.018 M KH_2PO_4 , 0.1 M NaCl, and 0.003 M KCl. All solutions were prepared using double deionized water (Millipore Corporation, Bedford, MA).

2.2. Device Fabrication. Source and drain electrodes were made with Au on a microporous luster photography-quality paper with a weight of 200 g/m^2 (Table S1), using an Orion RF magnetron sputtering (AJA International, MA; see the Supporting Information (SI) for experimental details). First, the photography paper was cut into a circle of 10 cm diameter (Figure S1-a) and then cleaned with ethanol and deionized water for 2 min successively, followed by drying with air. Next, parallel lines separated by an 8 mm gap were created on the paper by applying 0.5 mm wide strips of an adhesive masking tape (Figure S1-b) (ABC Hobby Co., Osaka, Japan). After sputtering 100 nm thick Au (Figure S1-c), the strips were removed, leaving a 0.5 mm wide gap between the gold pads, which will be the channel length, L . Finally, 0.8 cm \times 1.5 cm gold pads were cut to make the source and drain electrodes (Figure S1-d). An environmental scanning electron microscope (ESEM) (FEI Quanta 600) was used for characterization.

2.2.1. Drawing of the Channel by a Dip Pen Procedure. Different approaches, such as drop casting, dip coating, and dip pen deposition, were explored to apply PEDOT:PSS inks. The most reproducible results were obtained using a dip pen method. To draw the channel, we used standard tweezers (PELCO 5113 Carbofib Tip Tweezer) equipped with a 0.5 mm \times 0.6 mm (width \times thickness) carbon fiber tip (Figure S1-g). To this end, the tip was dipped into the pristine PEDOT:PSS solution and used to draw a fine line connecting the Au pads (Figure S1-e). The ink was dried in an oven at 100 $^\circ\text{C}$ for 20 min. Similarly, the second layer was made also by dipping the tip into

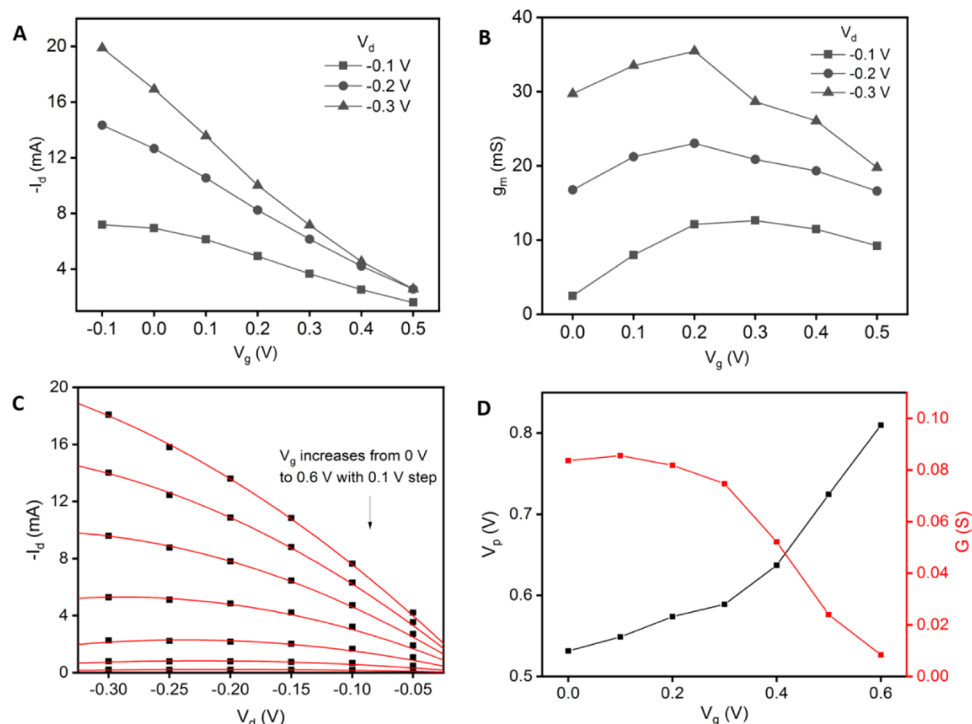


Figure 3. (A) Transfer curve, (B) transconductance, and (C) output curve (fitted using the Bernard–Malliaras model (red line)) of an OEET with a channel made of three PEDOT:PSS layers ($5.6 \mu\text{m}$ channel). (D) Pinch-off voltage and conductance calculated from the model.

the PEDOT:PSS ink and then drawing a line over the previous one. In this way, three and six layers were cast by repeating the same procedure. Thereafter, adhesive tape was used to cover the gold contacts, leaving only the PEDOT:PSS conductive channel exposed (Figure S1-f).

2.2.2. Construction of the Gate Electrodes. For the initial characterization of the system, a Ag/AgCl gate electrode (Warner Instruments LLC, MA) was used. For the detection of peroxide, the gate electrode was made by coating the paper Pt electrode with Nafion (Figure 1E), as described elsewhere.⁴⁰ In short, strips of the platinized paper ($0.4 \text{ cm} \times 2 \text{ cm}$) were sandwiched between two adhesive masks, leaving exposed only an electrochemical active window of 3 mm diameter. Then, $5 \mu\text{L}$ of the Nafion solution was sequentially drop-cast on this window and then left to dry overnight.³⁵ In the case of the detection of glucose, two drops of $5 \mu\text{L}$ of glucose oxidase solution (20 mg/mL in deionized water) were cast and dried at $4 \text{ }^\circ\text{C}$ for 6 h before drop-casting the Nafion.⁴¹

3. RESULTS AND DISCUSSION

3.1. Electrical Characterization of the Source/Drain System. Figure 2A,B shows the time trace and I_d – V_d plots for channels made with one, three, and six layers of the CP ink under dry conditions (i.e., before contact with an electrolyte solution). The time traces show stable values of currents and an ohmic behavior within the range tested (-0.2 to 0.2 V). This voltage range was limited for practical purposes to avoid currents higher than 20 mA. The dynamic resistance calculated from the slope of these plots (Table S2) shows that with the first layer, the system already shows a low resistance (in the order of 22Ω) that drops as more layers are added. For six layers, the resistance reaches a value of 11.0Ω . The overall value or the resistance measured is the result of the CP resistance and the contact resistance ($R_{\text{total}} = R_{\text{channel}} + R_{\text{contacts}}$).⁴² Gold pads are used to minimize the contact resistance with the electrodes, although it should be noted that some contact resistance might be also found between the

different layers of the CP, as reported by Pesavento et al. for pentacene-based thin-film transistors.⁴³

3.2. Characterization of Channel Thickness. Channel geometry, in particular, thickness,²⁹ is one of the main parameters affecting OEET performance. The most popular approaches to control the CP film thickness, spin coating and inkjet printing,⁵ require dedicated equipment and are more suitable for thin-film fabrication (below $1 \mu\text{m}$).⁴⁴ Ultrasimple methods such as dip pen, on the other hand, have been scarcely reported for fabrication of OEETs.^{45,46} In this work, the channel geometry is controlled through a simple approach. The length is set by the gap between the Au pad electrodes (0.5 mm). The width is determined by the size of the metallic tip used as a pen, which in this work creates a uniform width in the order of $1.00 \pm 0.04 \text{ mm}$. The channel thickness is mostly controlled by the rheological characteristics of the ink, which determines the pen loading, and also the interaction of the ink with the paper substrate, which determines the delivery of the CP ink. The cross-sectional images of the channel acquired with an environmental scanning electron microscope (ESEM) allow measuring the thickness of the PEDOT:PSS channel, as shown in Figures 2D–F. For one, three, and six layers, the final thicknesses of the channel were 2.55 ± 0.24 , 5.63 ± 0.14 , and $19.24 \pm 0.84 \mu\text{m}$, respectively. The error in the measurements shows that the film is reasonably uniform across the channel. Evidently, the thickness of the channel increases with the number of layers deposited. This growth, however, is not linear, since the thickness of the layer will depend on the delivery and the way the film dries. On average, the thickness has increased between 2 and $3 \mu\text{m}$ per applied layer. This is similar to inkjet printing of successive layers, which has been used in several works to control the thickness of thin films.⁴⁷ Therefore, multiple dip pen procedures could serve as a quick, simple, and low-cost alternative method to obtain thick-film channels. The stability and dynamic response of the channel

Table 1. Comparison of OEETs Characteristics

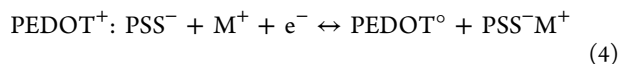
substrate	channel fabrication	gate material	channel material	W (μm)	L (μm)	T (μm)	g_m (mS)	voltages (V)	ref
PLA	3D printing	Ag/AgCl	PEDOT:PSS	912	694	7.1	31.8 ± 6.3	$V_d = -0.7$ $V_g = 0$	34
PE	printing	Ag/AgCl	PEDOT:PSS	1000	500	2.1	10	$V_d = -0.4$ $V_g = 0$	52
polyarylate	spin coating	Ag/AgCl	PEDOT:PSS/EMIM-TCM	1000	200	0.8	28.7	$V_d = -0.5$ $V_g = 0.42$	33
paper	dip pen	Ag/AgCl	PEDOT:PSS	1000	500	5.63	40.1 ± 3.6	$V_d = -0.3$ $V_g = 0.2$	This work
paper	dip pen	Pt/Nafion	PEDOT:PSS	1000	500	6	24.5	$V_d = -0.15$ $V_g = 0.2$	This work
Si wafer	spin coating	Au/PEDOT	PEDOT:PSS	500	5	6	32.3	$V_d = -0.6$ $V_g = 0.5$	4
glass	spin coating	Ag/AgCl	PEDOT:PSS	^a			142	$V_d = -0.6$ $V_g = 0.2$	50
PET	spin coating	Ag/AgCl	PEDOT:PSS	^b			139	$V_d = -0.6$ $V_g = 0.2$	51

^aPE: polyethylene, PLA: polylactic acid, EMIM-TCM: 1-ethyl-3-methylimidazolium tricyanomethanide. Interdigitated electrodes with finger number $N_f = 5$; finger width and channel length $W_f = L_{\text{ch}} = 5 \mu\text{m}$; and polymer film thickness $d = 115 \text{ nm}$. ^bInterdigitated electrodes (large comb) with finger number $N_f = 6$, channel length $L_{\text{ch}} = 8 \mu\text{m}$, and W/L ratio 230.

were tested by monitoring the current profile upon application of a square wave voltage at 0.05 Hz (50% duty cycle) during 40 cycles. In all cases, the rise and fall of the current is limited by the reading device, and it is below 1 s, well within the required performance (Figure S2).

3.3. Electrical Characterization of the OEET. Transistors were assembled by immersing the conducting channel and the Ag/AgCl gate electrode in a 0.1 M NaCl electrolyte solution. Once the voltage channel (V_d) was set, the current (I_d) was monitored as a function of time. The gate voltage bias (V_g) was modified from 0 to 0.9 V in 0.1 V increment steps that were applied each time I_d was stabilized. At the end of each run, the voltage was set back to zero to verify the return to the baseline. This process was repeated for a different V_d , and the transconductance (g_m) was calculated using eq 1. We have noted that our devices needed at least 100 s before I_d became stable. Therefore, the dwell time between points in the transfer and output curves (Figure 3) was set to 120 s.

Figure 3A shows the transfer curves (I_d vs V_g) for OEET with a $5.6 \mu\text{m}$ channel thickness (see Figure S3 for 2.5 and $19.2 \mu\text{m}$ channel thicknesses). The plots show that the initial I_d decreases as the gate voltage is increased, meaning that the transistor operates in depletion mode. This drop of I_d is caused by the injection of cations (Na^+) from the electrolyte into the PEDOT:PSS channel, which leads to a decrease in the concentration of charge carriers (holes) and a drop of the electrical conductivity of PEDOT. This process—the foundation of an OEET—is usually represented as⁴⁸



where M^+ is a cation injected from the electrolyte and PEDOT^+ and PEDOT^0 are the oxidized and reduced forms of the polymer, respectively. Transconductance (g_m) as a function of V_g and I_d vs V_d plots for different V_g can be seen in Figure 3B,C respectively. The results show that g_m increases with V_d and that it reaches a maximum at V_g approximately 0.2 V, which is within the ranges usually reported. It has been shown that this value depends on several factors, such as the nature of the gate and the geometrical relationships of the system.⁴⁹ In this work, g_m reaches a maximum value of $40.1 \pm 3.6 \text{ mS}$ (for $N = 4$ devices, see Figure S9-a,b). The profile of the normalized responses (Figure S9-c) indicates that the OEETs tested have similar properties. It should be stressed that the results shown correspond to a $5.6 \mu\text{m}$ channel, as it will be discussed below.

The minimum value of I_d , which represents the maximum de-doping of the channel, is reached at $V_g = 0.8 \text{ V}$, yielding an

on/off current ratio of 3.8×10^3 (Figure S2). Remarkably, these two values are among the highest figures reported for paper-based OEETs. Interestingly, good values of g_m can be obtained even at $V_g = 0 \text{ V}$, which may be useful in several applications.²⁶

The influence of channel thickness on g_m is shown in Figure 2C. Interestingly, channel thickness does not affect the conditions at which the maximum is reached ($V_g = 0.2 \text{ V}$). It is also worth noting that with three layers of CP, g_m reaches a maximum value and then levels off. This suggests that increasing the channel thickness beyond a certain critical value may be detrimental for performance, since factors such as response time and the on/off current ratio of the transistor may be negatively affected.³³ For instance, the time constants of two channels with three and six layers determined by applying a step gate voltage from 0 to 0.4 V at $V_d = -0.3 \text{ V}$ and fitting the response to an exponential function were 3.72 and 5.48 s, respectively (Figure S10).

The reasons for this behavior are not yet totally clear, although problems associated with film hydration, cation migration, etc. may be playing an important role. In short, the layers below $6 \mu\text{m}$ do not seem to effectively engage in the ion–electron coupling required in OEETs. Therefore, the following experiments were conducted using an OEET with a channel thickness of approximately $6 \mu\text{m}$, i.e., three layers of PEDOT:PSS.

It should be stressed that the values of g_m reported in this work are among the highest values reported for this type of devices. Table 1 compares the g_m values of this work with other state-of-the-art PEDOT:PSS OEETs, showing that, to the best of our knowledge, this is the highest transconductance reported for a paper-based OEET. Very recently, OEETs with high transconductance values have been also reported.^{50,51} It should be stressed that by tuning the film composition, drying procedures, substrate, and system geometry (e.g., gate to channel geometry), transconductances can be manipulated, sometimes at the expense of a more complex procedure. In the case of this work, a balance between performance and simplicity of manufacturing has been achieved. Satisfactory results have been obtained using the unmodified CP ink (i.e., as provided by the manufacturer) on a paper substrate with a simple construction approach.

3.4. Fundamental Parameters and the Volumetric Capacitance of the Channel. Accurate models describing the fundamental processes in OEETs are still a matter of intense research.⁵³ While the most evident difference with FET is the volumetric capacitance of OEETs,⁵⁴ Torsi and co-

workers have stressed that the fundamental physical phenomena are similar in both systems, but the main difference is where and how the electric double layer (EDL) is formed.⁵⁵ In an electrolyte-gated FET, the capacitance originates from the EDL created on the surface of an insulator material that separates the conducting polymer or/and the electrolyte. In OECT, on the other hand, the lack of this insulator material allows ions to move freely into the porous PEDOT:PSS structure. Thus, the capacitance originates on the EDL generated around the PEDOT domains. It has been shown that PEDOT forms dispersed micro- and nanostructured domains in a PSS–electrolyte matrix.²⁷ Therefore, the EDL is formed around these PEDOT domains, forming an extended and dispersed structure through the whole channel volume. In fact, the description of the OECT proposed by Bernardis et al.⁵⁶ is originally derived from the FET models,⁵⁷ providing that the interfacial (2D) capacitance is replaced by a volumetric (3D) capacitance. Therefore, the most commonly used model for an OECT in the depletion mode within the linear range, I_d , relates with the device geometry and the properties of the conducting polymer:

$$I_d = \frac{G}{V_p} \left(V_p - V_g + \frac{V_d}{2} \right) V_d \quad (5)$$

where G is the initial electrical conductance of the channel and V_p is the transistor pinch-off voltage, i.e., the value of V_g at which the system is almost fully de-doped. The fit of the experimental data to eq 5 using a least-squares method is shown in Figure 3D. The model provides a good fit to the data providing that—as reported by Alcácer et al.— G and V_p are used as variables. The channel conductance (G) shows an initial value of 84.5 mS (for $V_g = 0$ V), which is close to the initial value of resistance found for the channel (Figure 2C, although in this figure, the resistance is lower, since the channel is dry). The results of the models show that for V_g above 0.2 V, G decreases sharply and reaches a value of 8.7 mS for $V_g = 0.6$ V. Regarding the pinch-off voltage V_p , its value increases with V_g from 0.51 to 0.81 V, which is within the range of values that have been reported in the literature.

These results show that while thick-film OECTs present similar behavior to thin-film devices, they show particular features likely due to the deviations introduced by the increased channel thickness. In fact, the Bernardis–Malliaras model (eq 5), derived for homogeneous thin-film devices with uniform properties across the channel, has been under scrutiny during the last few years. Lüssem and co-workers have recently demonstrated that migration of ions toward the drain electrode produces gradients of concentration that affect the pinch voltage.⁵⁸ McLeod and co-workers have demonstrated the nonuniform mobility of holes in the PEDOT, a parameter that is assumed constant in the Bernardis–Malliaras model.⁵⁹ In summary, the generation of concentration and electrical field gradients, together with variations in the CP properties make the system more dependent on geometrical characteristics, particularly on film thickness. Studies on adaptations of the model to thicker films should be conducted in the future.

Rivnay et al. studied capacitance (C) as a function of channel volume, arriving to the following expression²⁹

$$C = C^* \times WLd \quad (6)$$

where C^* , the volumetric capacitance of the PEDOT:PSS channel, has a value of 40 F/cm³. Considering the volume of

the channel used in this work (with a volume of approximately 2.8×10^{-6} cm³), eq 6 predicts a capacitance of 112 μ F. Experimental measurements of the capacitance performed by impedance spectroscopy yield a value of capacitance of 106 μ F (Figure S5), which is fairly close to this value. The product of the charge carrier mobility and the volumetric capacitance ($\mu \cdot C^*$) has been proposed as a material's figure of merit for benchmarking OECTs.⁶⁰ For instance, the product ($\mu \cdot C^*$) extracted from fitting the Bernardis–Malliaras model to the output (Figure 3A,B) at $V_d = -0.3$ V and $V_g = 0$ V gives a value of 139.7 F/cm³·V·s, which is in agreement with the literature.^{16,60} Therefore, while models to accurately describe the behavior of thick-film OECTs will be required, the general properties of these devices match those of the thin-film counterparts. The thick-film technology, however, provides a simplified manufacturing approach and enhanced response.

3.5. Detection of H₂O₂. To illustrate the advantages of thick-film transistors, a system for the detection of hydrogen peroxide was built and optimized. This molecule is widely used in biochemical sensing as an intermediary species for signal generation. During the last few years, we reported the sensitive and selective potentiometric determination of H₂O₂ using a Pt electrode coated with Nafion. Interestingly, while often referred to as a redox reaction of peroxide, however, the response of the Pt electrode is due to a mixed potential mechanism involving exchange currents from different surface reactions, mainly the oxygen reduction reaction and the Pt oxidation.⁶¹ Thus, the potentiometric measurement does not follow a Nernstian regime, since the kinetically controlled surface reactions create concentration gradients on the electrode. Nafion enhances these surface reactions, preventing the adsorption of interfering anions, providing reactive species, and stabilizing the electrode response.³⁵ Furthermore, its biocompatibility is ideal for the development of biosensors.⁶²

An OECT was built using a channel with three layers of PEDOT:PSS ($W = 1$ mm and $L = 0.5$ mm) and a paper-based Nafion-coated Pt electrode as a gate. Conditions were optimized to maximize the sensitivity of the detection. V_d was adjusted to -0.3 V to keep I_{SD} below 20 mA. The use of Pt electrode introduces a new variable in the system. Ag/AgCl electrodes show a negligible capacitance, so the applied gate potential is similar to the effective gate potential. In the case of the Pt/Nafion electrode, however, the effective gate potential (V_g^{eff}) is different from the applied gate potential, since the electrode capacitance and the redox potential have to be also considered. In fact, this is the working principle of the sensor: alterations in the concentration of an electroactive species (H₂O₂) that affect the effective gate potential will be registered as changes in I_d . In this case, eq 5 can be rewritten as

$$I_d = \frac{G}{V_p} \left(V_p - V_g^{\text{eff}} + \frac{1}{2} \times V_d \right) V_d \quad (7)$$

where

$$V_g^{\text{eff}} = V_g + V_{\text{offset}}$$

The term V_{offset} includes the capacitances at the interfaces and the redox potential of the system. Initial tests (data not shown) show that, in the absence of Pt, PEDOT shows a negligible response to peroxide. When adding peroxide with a Pt gate, however, the change in the potential of the Pt electrode is registered as a drop in the channel current. The optimization was performed by evaluating the sensitivity for the detection of

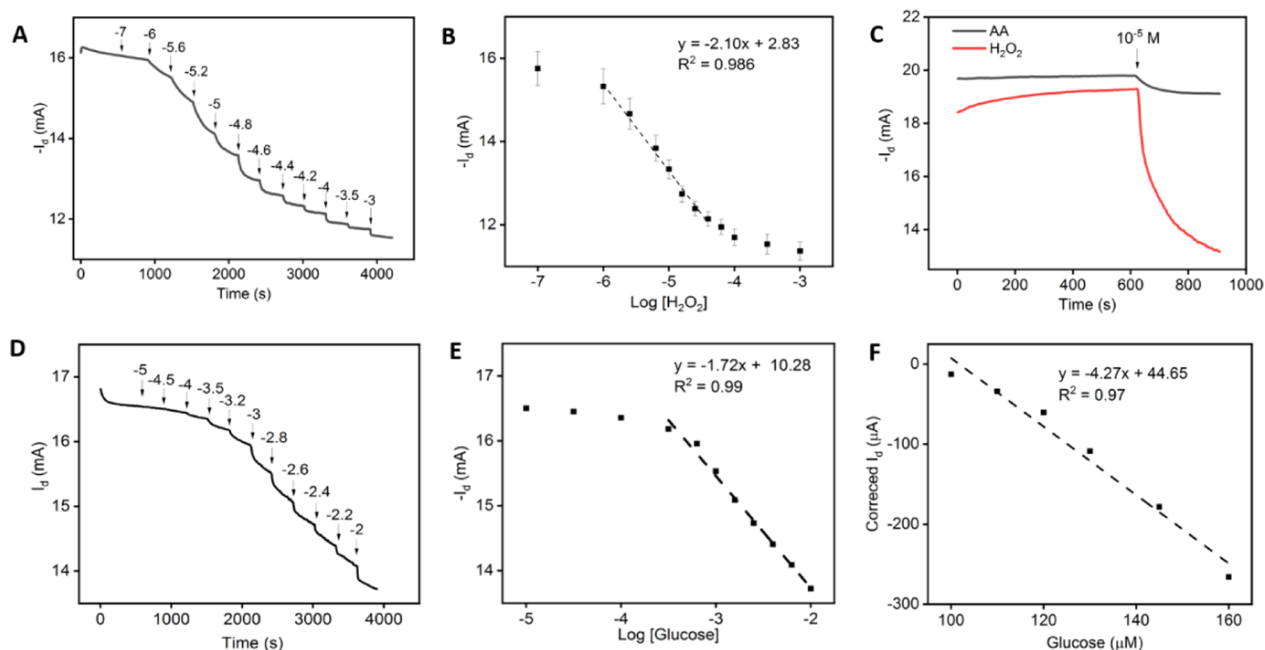


Figure 4. (A) Time trace of the OECT response for increasing concentrations of H_2O_2 (numbers indicate logarithmic concentrations of the target). (B) Corresponding logarithmic calibration curve (the error bars correspond to standard deviation of three sensors). (C) Response of a sensor to ascorbic acid (AA) and H_2O_2 . (D) Time trace of an OECT response for increasing concentrations of glucose. (E) Corresponding logarithmic calibration curve. (F) Calibration curve corresponding to a 100–160 μM range. In all cases, OECT is operated at $V_d = -0.3$ V and $V_g = 0.2$ V. The numbers on the time traces represent the logarithm of the concentration of the analyte.

Table 2. Comparison of the Analytical Performances of Different H_2O_2 and Glucose OECT-Based Sensors^a

channel	analyte	gate	W (mm)	L (mm)	sensitivity	LOD (μM)	LR	ref
PEDOT	H_2O_2	PtNP/MWCNT /CPE	6	0.12	0.234 NCR	0.2	0.5 μM –0.1 mM	36
graphene	H_2O_2	PtNP/graphene	3	0.2	91.7 mV/dec	0.03	3–300 μM	17
PEDOT	H_2O_2	Pt/Nafion	1	0.5	2.1 mA/dec	0.3	1–40 μM	this work
PEDOT	glucose	CHIT–graphene/GOx/Pt	6	0.2	370 mV/dec	0.01	10 nM–1 μM	63
graphene	glucose	GOx-CHIT/Nafion/PtNPs/graphene	3	0.2	173 mV/dec	0.5	≈ 10 μM –8 mM	17
PEDOT	glucose	Au/PEDOT/PtNP/CHIT/GOx			0.4762 NCR		10–700 μM	64
PEDOT	glucose	Pt/GOx/Nafion	1	0.5	1.72 mA/dec	100	300 μM –10 mM	this work

^aLOD: limit of detection; LR: linear range.

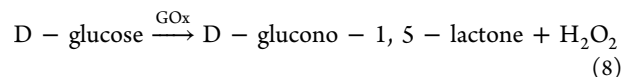
peroxide at different gate potentials. Optimum conditions were found for $V_g = 0.2$ V and $V_d = -0.3$ V (Figure S6). The time trace of I_d upon addition of peroxide is shown in Figure 4A, and the corresponding calibration plot is shown in Figure 4B.

The sensor displays a linear response with the logarithm of the concentration of peroxide in the range 10^{-6} – $10^{-4.4}$ M. Under optimum conditions, an outstanding sensitivity of 2.1 mA/dec is reached. This value is several orders of magnitude higher than the values reported for other similar sensors. For comparison, selected examples of OECTs reported sensitivity are shown in Table 2. In this work, the limit of detection is 3×10^{-7} M. While this system has not been optimized to improve the limit of detection, the value obtained is comparable to thin-film OECTs³⁶ and 1 order of magnitude higher than graphene-based OECT.³⁶

On the other hand, ascorbic acid (AA) is known to interfere with the electrochemical detection of H_2O_2 . Figure 4C shows the limited response of the sensor to the addition of 10^{-5} M of ascorbic acid, a concentration that is usually considered an upper level in physiological samples. As can be observed, for the same concentration added, the change in the drain current caused by AA is significantly lower than the response to H_2O_2 . This low response toward AA is attributed to the presence of

the anionic groups on Nafion, which acts as a permselective barrier repelling the negatively charged AA and enhancing the detection of H_2O_2 .

3.6. Detection of Glucose. As a way to illustrate the use of the thick film for biosensing, glucose oxidase (GOx) enzyme was added to the Pt-Nafion gate. GOx acts as a catalyst for the oxidation of glucose according to



In this reaction, H_2O_2 is a byproduct that alters the potential of the platinum electrode, causing a change in the channel conductivity, as discussed above. The time trace with the response of the sensor to increasing concentration of glucose is shown in Figure 4D, and the corresponding calibration curve is shown in Figure 4E. The sensitivity in this case is 1.72 mA/dec, and the limit of detection is 1.10×10^{-4} M. The linear range spans from $10^{-3.5}$ to 10^{-2} M. These values are acceptable to cover, for example, the normal range of glucose in blood. Optimization of these values can be achieved by modifying the gate characteristics. Linear ranges, for example, can be adjusted by replacing Nafion with other ionomeric materials.⁶⁵ The

limit of detection can be further improved by optimizing the area of the gate as well as the volume and concentration of the Nafion/GOx deposited.⁴¹ Moreover, the integration of Pt nanoparticles, CNT, and/or graphene in the gate electrode has proven to enhance the limit of detection and shift the linear range toward small concentrations of glucose (Table 2).^{17,66} All this will depend on the type of biological fluid that will be target.

To validate the specificity of the response, the response to glucose of an OECT without GOx was evaluated, and the response is shown in Figure S7. The first part of this figure shows the initial drop of current produced by setting the gate at 0.2 V. This is a rather large potential step, and for that reason, stabilization time is relatively long. After that, the GOx-free sensor does not show any significant response to the addition of three concentrations of glucose, 10^{-5} , 10^{-4} , and 10^{-3} M.

Clearly, with enhanced sensitivity and response time in the order of tens of seconds, these thick-film transistors offer a valuable approach for chemical and biochemical sensing. In terms of detectability, they offer enhanced sensitivity due to the power amplification provided by OECTs. In a very recent work regarding this topic, Malliaras et al. discussed the issues of thickness and noise level, concluding—in line with this work—that channel thickness should be increased as much as allowed by the response time.⁶⁷ In this work, currents in the order of a few milliamperes show noise levels in the single μA range (typically, a 10 mA current shows a standard deviation of 2×10^{-3} mA). Figures 4F and S8 show a calibration plot between 100 and 160 μM of glucose, illustrating the enhanced power of detection provided by the high sensitivity of the OECT, i.e., $4.27 \mu\text{A}/\mu\text{M}$. These values can be improved considering that the noise observed is heavily influenced by the ripple of the commercial, low-cost power supplies used. In fact, using a stabilized DC power supply, the standard deviation of I_d can go down below 8×10^{-5} mA. Considering sensitivities of 2 mA/decade, this noise level provides a very attractive signal-to-noise ratio. Alternatively, it has been shown that simple approaches to signal amplification, such as the use of a load resistor, can provide significant signal improvements. It should be stressed that the traditional potentiometric methods working under zero current conditions (i.e., currents well below picoamperes), signals of a few hundreds of millivolts, will result in signals well below nano- or picowatt power. The significantly higher power of the OECT signals provides room for signal enhancement.

4. CONCLUSIONS

This work has shown several advantages arising from the use of thick-film OECT chemical sensors. First, the high transconductance achieved by these devices provides enhanced analytical figures, such as high sensitivity and signal-to-noise ratio. Second, the practical advantages of a low-cost and simple manufacturing approach. The possibility to build manually reproducible paper-based OECT sensors facilitates their adoption and further exploration. In summary, these paper-based thick-film OECTs open new and attractive avenues for the development of highly sensitive, powerful, simple, and low-cost chemical and biochemical sensors.

■ ASSOCIATED CONTENT

Supporting Information

The Supporting Information is available free of charge at <https://pubs.acs.org/doi/10.1021/acsaelm.1c00116>.

Instrumentation, electrical characterization, sputtering conditions, transfer curves, and electrochemical impedance analysis (PDF)

■ AUTHOR INFORMATION

Corresponding Author

Francisco J. Andrade – Department of Analytical and Organic Chemistry, Universitat Rovira i Virgili, 43007 Tarragona, Spain; orcid.org/0000-0003-1199-2837; Email: franciscojavier.andrade@urv.cat

Authors

Adil Ait Yazza – Department of Analytical and Organic Chemistry, Universitat Rovira i Virgili, 43007 Tarragona, Spain

Pascal Blondeau – Department of Analytical and Organic Chemistry, Universitat Rovira i Virgili, 43007 Tarragona, Spain; orcid.org/0000-0003-1331-5055

Complete contact information is available at: <https://pubs.acs.org/doi/10.1021/acsaelm.1c00116>

Author Contributions

The manuscript was written through contributions of all authors. All authors have given approval to the final version of the manuscript.

Notes

The authors declare no competing financial interest.

■ ACKNOWLEDGMENTS

The authors acknowledge the financial support from the Spanish ministry of Economy and Competitiveness and European Regional Development Fund (ERDF) (Project CTQ2016-77128-R and PID2019-106862RB-I00).

■ REFERENCES

- (1) Kittlesen, G. P.; White, H. S.; Wrighton, M. S. Chemical Derivatization of Microelectrode Arrays by Oxidation of Pyrrole and N-Methylpyrrole: Fabrication of Molecule-Based Electronic Devices. *J. Am. Chem. Soc.* **1984**, *106*, 7389–7396.
- (2) Rivnay, J.; Inal, S.; Salleo, A.; Owens, R. M.; Berggren, M.; Malliaras, G. G. Organic Electrochemical Transistors. *Nat. Rev. Mater.* **2018**, *3*, No. 17086.
- (3) Majak, D.; Fan, J.; Gupta, M. Fully 3D Printed OECT Based Logic Gate for Detection of Cation Type and Concentration. *Sens. Actuators, B* **2019**, *286*, 111–118.
- (4) Spyropoulos, G. D.; Gelinis, J. N.; Khodagholy, D. Internal Ion-Gated Organic Electrochemical Transistor: A Building Block for Integrated Bioelectronics. *Sci. Adv.* **2019**, *5*, No. eaau7378.
- (5) Lin, P.; Yan, F. Organic Thin-Film Transistors for Chemical and Biological Sensing. *Adv. Mater.* **2012**, *24*, 34–51.
- (6) Wen, Y.; Xu, J. Scientific Importance of Water-Processable PEDOT-PSS and Preparation, Challenge and New Application in Sensors of Its Film Electrode: A Review. *J. Polym. Sci., Part A: Polym. Chem.* **2017**, *55*, 1121–1150.
- (7) Bihar, E.; Deng, Y.; Miyake, T.; Saadaoui, M.; Malliaras, G. G.; Rolandi, M. A Disposable Paper Breathalyzer with an Alcohol Sensing Organic Electrochemical Transistor. *Sci. Rep.* **2016**, *6*, No. 27582.
- (8) Zhang, S.; Ling, H.; Chen, Y.; Cui, Q.; Ni, J.; Wang, X.; Hartel, M. C.; Meng, X.; Lee, K.; Lee, J.; Sun, W.; Lin, H.; Emaminejad, S.; Ahadian, S.; Ashammakhi, N.; Dokmeci, M. R.; Khademhosseini, A.

Hydrogel-Enabled Transfer-Printing of Conducting Polymer Films for Soft Organic Bioelectronics. *Adv. Funct. Mater.* **2020**, *30*, No. 1906016.

(9) Lin, P.; Luo, X.; Hsing, I. M.; Yan, F. Organic Electrochemical Transistors Integrated in Flexible Microfluidic Systems and Used for Label-Free DNA Sensing. *Adv. Mater.* **2011**, *23*, 4035–4040.

(10) Zhang, S.; Hubis, E.; Tomasello, G.; Soliveri, G.; Kumar, P.; Cicoira, F. Patterning of Stretchable Organic Electrochemical Transistors. *Chem. Mater.* **2017**, *29*, 3126–3132.

(11) Matsuhisa, N.; Jiang, Y.; Liu, Z.; Chen, G.; Wan, C.; Kim, Y.; Kang, J.; Tran, H.; Wu, H.; You, I.; Bao, Z.; Chen, X. High-Transconductance Stretchable Transistors Achieved by Controlled Gold Microcrack Morphology. *Adv. Electron. Mater.* **2019**, *5*, No. 1900347.

(12) Zhang, S.; Li, Y.; Tomasello, G.; Anthonisen, M.; Li, X.; Mazzeo, M.; Genco, A.; Grutter, P.; Cicoira, F. Tuning the Electromechanical Properties of PEDOT:PSS Films for Stretchable Transistors And Pressure Sensors. *Adv. Electron. Mater.* **2019**, *5*, No. 1900191.

(13) Gualandi, I.; Marzocchi, M.; Achilli, A.; Cavedale, D.; Bonfiglio, A.; Fraboni, B. Textile Organic Electrochemical Transistors as a Platform for Wearable Biosensors. *Sci. Rep.* **2016**, *6*, No. 33637.

(14) Cicoira, F.; Sessolo, M.; Yaghmazadeh, O.; DeFranco, J. A.; Yang, S. Y.; Malliaras, G. G. Influence of Device Geometry on Sensor Characteristics of Planar Organic Electrochemical Transistors. *Adv. Mater.* **2010**, *22*, 1012–1016.

(15) Friedlein, J. T.; McLeod, R. R.; Rivnay, J. Device Physics of Organic Electrochemical Transistors. *Org. Electron.* **2018**, *63*, 398–414.

(16) Colucci, R.; Barbosa, H. F. D. P.; Günther, F.; Cavassin, P.; Faria, G. C. Recent Advances in Modeling Organic Electrochemical Transistors. *Flex. Print. Electron.* **2020**, *5*, No. 013001.

(17) Zhang, M.; Liao, C.; Mak, C. H.; You, P.; Mak, C. L.; Yan, F. Highly Sensitive Glucose Sensors Based on Enzyme-Modified Whole-Graphene Solution-Gated Transistors. *Sci. Rep.* **2015**, *5*, No. 8311.

(18) Gualandi, I.; Tonelli, D.; Mariani, F.; Scavetta, E.; Marzocchi, M.; Fraboni, B. Selective Detection of Dopamine with an All PEDOT:PSS Organic Electrochemical Transistor. *Sci. Rep.* **2016**, *6*, No. 35419.

(19) Liao, C.; Mak, C.; Zhang, M.; Chan, H. L. W.; Yan, F. Flexible Organic Electrochemical Transistors for Highly Selective Enzyme Biosensors and Used for Saliva Testing. *Adv. Mater.* **2015**, *27*, 676–681.

(20) Gualandi, I.; Marzocchi, M.; Scavetta, E.; Calienni, M.; Bonfiglio, A.; Fraboni, B. A Simple All-PEDOT:PSS Electrochemical Transistor for Ascorbic Acid Sensing. *J. Mater. Chem. B* **2015**, *3*, 6753–6762.

(21) Hu, J.; Wei, W.; Ke, S.; Zeng, X.; Lin, P. A Novel and Sensitive Sarcosine Biosensor Based on Organic Electrochemical Transistor. *Electrochim. Acta* **2019**, *307*, 100–106.

(22) Gentili, D.; D'Angelo, P.; Militano, F.; Mazzei, R.; Poerio, T.; Bruciale, M.; Tarabella, G.; Bonetti, S.; Marasso, S. L.; Cocuzza, M.; Giorno, L.; Iannotta, S.; Cavallini, M. Integration of Organic Electrochemical Transistors and Immuno-Affinity Membranes for Label-Free Detection of Interleukin-6 in the Physiological Concentration Range through Antibody–Antigen Recognition. *J. Mater. Chem. B* **2018**, *6*, 5400–5406.

(23) Yeung, S. Y.; Gu, X.; Tsang, C. M.; Tsao, S. W.; Hsing, I. Engineering Organic Electrochemical Transistor (OECT) to Be Sensitive Cell-Based Biosensor through Tuning of Channel Area. *Sens. Actuators, A* **2019**, *287*, 185–193.

(24) Hai, W.; Goda, T.; Takeuchi, H.; Yamaoka, S.; Horiguchi, Y.; Matsumoto, A.; Miyahara, Y. Human Influenza Virus Detection Using Sialyllactose-Functionalized Organic Electrochemical Transistors. *Sens. Actuators, B* **2018**, *260*, 635–641.

(25) Qing, X.; Wang, Y.; Zhang, Y.; Ding, X.; Zhong, W.; Wang, D.; Wang, W.; Liu, Q.; Liu, K.; Li, M.; Lu, Z. Wearable Fiber-Based Organic Electrochemical Transistors as a Platform for Highly

Sensitive Dopamine Monitoring. *ACS Appl. Mater. Interfaces* **2019**, *11*, 13105–13113.

(26) Rivnay, J.; Leleux, P.; Sessolo, M.; Khodagholy, D.; Hervé, T.; Fiocchi, M.; Malliaras, G. G. Organic Electrochemical Transistors with Maximum Transconductance at Zero Gate Bias. *Adv. Mater.* **2013**, *25*, 7010–7014.

(27) Volkov, A. V.; Wijeratne, K.; Mitraka, E.; Ail, U.; Zhao, D.; Tybrandt, K.; Andreasen, J. W.; Berggren, M.; Crispin, X.; Zozoulenko, I. V. Understanding the Capacitance of PEDOT:PSS. *Adv. Funct. Mater.* **2017**, *27*, No. 1700329.

(28) Khodagholy, D.; Rivnay, J.; Sessolo, M.; Gurfinkel, M.; Leleux, P.; Jimison, L. H.; Stavrinidou, E.; Herve, T.; Sanaur, S.; Owens, R. M.; Malliaras, G. G. High Transconductance Organic Electrochemical Transistors. *Nat. Commun.* **2013**, *4*, No. 2133.

(29) Rivnay, J.; Leleux, P.; Ferro, M.; Sessolo, M.; Williamson, A.; Koutsouras, D. A.; Khodagholy, D.; Ramuz, M.; Strakosas, X.; Owens, R. M.; Benar, C.; Badier, J. M.; Bernard, C.; Malliaras, G. G. High-Performance Transistors for Bioelectronics through Tuning of Channel Thickness. *Sci. Adv.* **2015**, *1*, No. e1400251.

(30) Khodagholy, D.; Rivnay, J.; Sessolo, M.; Gurfinkel, M.; Leleux, P.; Jimison, L. H.; Stavrinidou, E.; Herve, T.; Sanaur, S.; Owens, R. M.; Malliaras, G. G. High Transconductance Organic Electrochemical Transistors. *Nat. Commun.* **2013**, *4*, No. 2133.

(31) Wang, N.; Yang, A.; Fu, Y.; Li, Y.; Yan, F. Functionalized Organic Thin Film Transistors for Biosensing. *Acc. Chem. Res.* **2019**, *52*, 277–287.

(32) Spyropoulos, G. D.; Gelinis, J. N.; Khodagholy, D. Internal Ion-Gated Organic Electrochemical Transistor: A Building Block for Integrated Bioelectronics. *Sci. Adv.* **2019**, *5*, No. eaau7378.

(33) Wu, X.; Surendran, A.; Ko, J.; Filonik, O.; Herzig, E. M.; Müller-Buschbaum, P.; Leong, W. L. Ionic-Liquid Doping Enables High Transconductance, Fast Response Time, and High Ion Sensitivity in Organic Electrochemical Transistors. *Adv. Mater.* **2019**, *31*, No. 1805544.

(34) Fan, J.; Montemagno, C.; Gupta, M. 3D Printed High Transconductance Organic Electrochemical Transistors on Flexible Substrates. *Org. Electron.* **2019**, *73*, 122–129.

(35) Parrilla, M.; Cánovas, R.; Andrade, F. J. Enhanced Potentiometric Detection of Hydrogen Peroxide Using a Platinum Electrode Coated with Nafion. *Electroanalysis* **2017**, *29*, 223–230.

(36) Guo, X.; Cao, Q.; Liu, Y.; He, T.; Liu, J.; Huang, S.; Tang, H.; Ma, M. Organic Electrochemical Transistor for in Situ Detection of H₂O₂ Released from Adherent Cells and Its Application in Evaluating the in Vitro Cytotoxicity of Nanomaterial. *Anal. Chem.* **2020**, *92*, 908–915.

(37) Tang, H.; Yan, F.; Lin, P.; Xu, J.; Chan, H. L. W. Highly Sensitive Glucose Biosensors Based on Organic Electrochemical Transistors Using Platinum Gate Electrodes Modified with Enzyme and Nanomaterials. *Adv. Funct. Mater.* **2011**, *21*, 2264–2272.

(38) Liao, J.; Lin, S.; Yang, Y.; Liu, K.; Du, W. Highly Selective and Sensitive Glucose Sensors Based on Organic Electrochemical Transistors Using TiO₂ Nanotube Arrays-Based Gate Electrodes. *Sens. Actuators, B* **2015**, *208*, 457–463.

(39) Pappa, A. M.; Curto, V. F.; Braendlein, M.; Strakosas, X.; Donahue, M. J.; Fiocchi, M.; Malliaras, G. G.; Owens, R. M. Organic Transistor Arrays Integrated with Finger-Powered Microfluidics for Multianalyte Saliva Testing. *Adv. Healthcare Mater.* **2016**, *5*, 2295–2302.

(40) Guadarrama-Fernández, L.; Novell, M.; Blondeau, P.; Andrade, F. J. A Disposable, Simple, Fast and Low-Cost Paper-Based Biosensor and Its Application to the Determination of Glucose in Commercial Orange Juices. *Food Chem.* **2018**, *265*, 64–69.

(41) Parrilla, M.; Cánovas, R.; Andrade, F. J. Paper-Based Enzymatic Electrode with Enhanced Potentiometric Response for Monitoring Glucose in Biological Fluids. *Biosens. Bioelectron.* **2017**, *90*, 110–116.

(42) Kaphle, V.; Liu, S.; Al-Shadeedi, A.; Keum, C.-M.; Lüssem, B. Contact Resistance Effects in Highly Doped Organic Electrochemical Transistors. *Adv. Mater.* **2016**, *28*, 8766–8770.

- (43) Pesavento, P. V.; Puntambekar, K. P.; Frisbie, C. D.; McKeen, J. C.; Ruden, P. P. Film and Contact Resistance in Pentacene Thin-Film Transistors: Dependence on Film Thickness, Electrode Geometry, and Correlation with Hole Mobility. *J. Appl. Phys.* **2006**, *99*, No. 094504.
- (44) Kholghi Eshkalak, S.; Chinnappan, A.; Jayathilaka, W. A. D. M.; Khatibzadeh, M.; Kowsari, E.; Ramakrishna, S. A Review on Inkjet Printing of CNT Composites for Smart Applications. *Appl. Mater. Today* **2017**, *9*, 372–386.
- (45) Minary, T.; Kanehara, Y.; Liu, C.; Sakamoto, K.; Yasuda, T.; Yaguchi, A.; Tsukada, S.; Kashizaki, K.; Kanehara, M. Room-Temperature Printing of Organic Thin-Film Transistors with π -Junction Gold Nanoparticles. *Adv. Funct. Mater.* **2014**, *24*, 4886–4892.
- (46) Cho, J.; Cheon, K. H.; Ahn, H.; Park, K. H.; Kwon, S.-K.; Kim, Y.-H.; Chung, D. S. High Charge-Carrier Mobility of $2.5 \text{ cm}^2 \text{ V}^{-1} \text{ s}^{-1}$ from a Water-Borne Colloid of a Polymeric Semiconductor via Smart Surfactant Engineering. *Adv. Mater.* **2015**, *27*, 5587–5592.
- (47) Moya, A.; Gabriel, G.; Villa, R.; Javier del Campo, F. Inkjet-Printed Electrochemical Sensors. *Curr. Opin. Electrochem.* **2017**, *3*, 29–39.
- (48) Robinson, N. D.; Svensson, P.-O.; Nilsson, D.; Berggren, M. On the Current Saturation Observed in Electrochemical Polymer Transistors. *J. Electrochem. Soc.* **2006**, *153*, H39.
- (49) Hütter, P. C.; Rothländer, T.; Haase, A.; Trimmel, G.; Stadlober, B. Influence of Geometry Variations on the Response of Organic Electrochemical Transistors. *Appl. Phys. Lett.* **2013**, *103*, No. 043308.
- (50) Liang, Y.; Brings, F.; Maybeck, V.; Ingebrandt, S.; Wolftrum, B.; Pich, A.; Offenhäusser, A.; Mayer, D. Tuning Channel Architecture of Interdigitated Organic Electrochemical Transistors for Recording the Action Potentials of Electrogenic Cells. *Adv. Funct. Mater.* **2019**, *29*, No. 1902085.
- (51) Tyrrell, J. E.; Boutelle, M. G.; Campbell, A. J. Measurement of Electrophysiological Signals In Vitro Using High-Performance Organic Electrochemical Transistors. *Adv. Funct. Mater.* **2021**, *31*, No. 2007086.
- (52) Romele, P.; Ghittorelli, M.; Kovács-Vajna, Z. M.; Torricelli, F. Ion Buffering and Interface Charge Enable High Performance Electronics with Organic Electrochemical Transistors. *Nat. Commun.* **2019**, *10*, No. 3044.
- (53) Colucci, R.; de Paula Barbosa, H. F.; Günther, F.; Cavassin, P.; Faria, G. C. Recent Advances in Modeling Organic Electrochemical Transistors. *Flex. Print. Electron.* **2020**, *5*, No. 013001.
- (54) Proctor, C. M.; Rivnay, J.; Malliaras, G. G. Understanding Volumetric Capacitance in Conducting Polymers. *J. Polym. Sci., Part B: Polym. Phys.* **2016**, *54*, 1433–1436.
- (55) MacChia, E.; Picca, R. A.; Manoli, K.; Di Franco, C.; Blasi, D.; Sarcina, L.; Ditaranto, N.; Cioffi, N.; Österbacka, R.; Scamarcio, G.; Torricelli, F.; Torsi, L. About the Amplification Factors in Organic Bioelectronic Sensors. *Mater. Horiz.* **2020**, *7*, 999–1013.
- (56) Bernards, D. A.; Malliaras, G. G. Steady-State and Transient Behavior of Organic Electrochemical Transistors. *Adv. Funct. Mater.* **2007**, *17*, 3538–3544.
- (57) Torsi, L.; Magliulo, M.; Manoli, K.; Palazzo, G. Organic Field-Effect Transistor Sensors: A Tutorial Review. *Chem. Soc. Rev.* **2013**, *42*, 8612–8628.
- (58) Kaphle, V.; Paudel, P. R.; Dahal, D.; Radha Krishnan, R. K.; Lüssem, B. Finding the Equilibrium of Organic Electrochemical Transistors. *Nat. Commun.* **2020**, *11*, No. 2515.
- (59) Friedlein, J. T.; Shaheen, S. E.; Malliaras, G. G.; McLeod, R. R. Optical Measurements Revealing Nonuniform Hole Mobility in Organic Electrochemical Transistors. *Adv. Electron. Mater.* **2015**, *1*, No. 1500189.
- (60) Inal, S.; Malliaras, G. G.; Rivnay, J. Benchmarking Organic Mixed Conductors for Transistors. *Nat. Commun.* **2017**, *8*, No. 1767.
- (61) Baez, J. F.; Compton, M.; Chahrahi, S.; Cánovas, R.; Blondeau, P.; Andrade, F. J. Controlling the Mixed Potential of Polyelectrolyte-Coated Platinum Electrodes for the Potentiometric Detection of Hydrogen Peroxide. *Anal. Chim. Acta* **2020**, *1097*, 204–213.
- (62) Kim, G.; Kim, H.; Kim, I. J.; Kim, J. R.; Lee, J. I.; Ree, M. Bacterial Adhesion, Cell Adhesion and Biocompatibility of Nafion Films. *J. Biomater. Sci., Polym. Ed.* **2009**, *20*, 1687–1707.
- (63) Liao, C.; Zhang, M.; Niu, L.; Zheng, Z.; Yan, F. Highly Selective and Sensitive Glucose Sensors Based on Organic Electrochemical Transistors with Graphene-Modified Gate Electrodes. *J. Mater. Chem. B* **2013**, *1*, 3820–3829.
- (64) Diacci, C.; Lee, J. W.; Janson, P.; Dufil, G.; Méhes, G.; Berggren, M.; Simon, D. T.; Stavrinidou, E. Real-Time Monitoring of Glucose Export from Isolated Chloroplasts Using an Organic Electrochemical Transistor. *Adv. Mater. Technol.* **2020**, *5*, No. 1900262.
- (65) Cánovas, R.; Blondeau, P.; Andrade, F. J. Modulating the Mixed Potential for Developing Biosensors: Direct Potentiometric Determination of Glucose in Whole, Undiluted Blood. *Biosens. Bioelectron.* **2020**, *163*, No. 112302.
- (66) Liao, C.; Zhang, M.; Niu, L.; Zheng, Z.; Yan, F. Highly Selective and Sensitive Glucose Sensors Based on Organic Electrochemical Transistors with Graphene-Modified Gate Electrodes. *J. Mater. Chem. B* **2013**, *1*, 3820.
- (67) Polyravas, A. G.; Schaefer, N.; Curto, V. F.; Calia, A. B.; Guimera-Brunet, A.; Garrido, J. A.; Malliaras, G. G. Effect of Channel Thickness on Noise in Organic Electrochemical Transistors. *Appl. Phys. Lett.* **2020**, *117*, No. 073302.